Engineering Structures 333 (2025) 120188

Contents lists available at ScienceDirect

Engineering Structures

journal homepage: www.elsevier.com/locate/engstruct

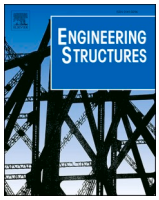

Influence of gravity load trapezes in the seismic performance of suspended piping systems

Derek Rodriguez [a,*], Daniele Perrone [b], Andre Filiatrault [a,1]

[a] University School for Advanced Studies IUSS, Pavia, Italy
[b] University of Salento, Italy

ARTICLE INFO

Keywords:
Non-structural elements
Nonstructural components
Suspended piping systems
Hangers
Seismic performance
Fragility
Gravity load trapezes

ABSTRACT

Non-structural elements play a critical role in the post-earthquake functionality of code-compliant and emergency management facilities. Poor seismic performance of suspended piping systems has been documented in the aftermath of recent seismic events in urban regions, which hindered the continuous operation of several buildings and facilities. The seismic design of such systems usually consists of installing channel or rod braces to minimize the swaying of the suspended pipes and increase the lateral stiffness of the gravity load supports, which typically are channel or rod trapezes. One common assumption made when analysing and designing suspended piping systems, is that the lateral stiffness of the gravity load trapezes, often referred to as hangers, is negligible in comparison with that of the sway-braced trapezes, resulting in the sway-braced trapezes being designed to sustain the totality of the seismic loads. This paper presents the results of a numerical study that investigated the influence of the gravity load trapezes of seismically designed suspended piping systems on their seismic performance. Two different suspended piping layouts using channel trapezes installed in four different reinforced concrete moment-resisting frames were investigated under two conditions: i) neglecting the lateral stiffness of the gravity load trapezes, and ii) assuming an elastic-perfectly plastic behaviour for the gravity load trapezes consistent with the material and section properties provided by the manufacturer technical specifications. The results are compared by means of fragility curves for various performance objectives and recommendations are given.

1. Introduction

Several typologies of non-structural elements (NSEs) have exhibited a poor seismic performance after recent seismic events that have occurred in the vicinity of large urban regions. Additionally, several loss estimation studies conducted in existing buildings have highlighted that the expected losses related to NSEs are generally higher than the losses associated to the structural elements [1,2]. As a result, the seismic performance of NSEs has become a crucial aspect of the performance-based earthquake engineering framework [3]. Some of the key issues that contributes to the poor seismic performance of NSEs are the highly empirical nature of their seismic design provisions, and the higher vulnerability that they exhibit in comparison with their structural counterpart, specially at lower seismic intensities.

Post-earthquake functionality of critical facilities is a key issue when it comes to emergency management in the aftermath of a seismic event. Poor seismic performance of NSEs has been identified as an impediment for the continuous operation of buildings and facilities. For piping systems, the damage documented following recent seismic events has demonstrated their high vulnerability and influence in the post-earthquake functionality of buildings. For example, in the aftermath of the 2010 Chile earthquake, several airports and hospitals saw their functionality partially reduced due to damage experienced by suspended piping and fire suppression systems [4]. During the 1994 Northridge earthquake in California, several buildings had to be temporarily evacuated as a result of the leakage and water damage resulting from piping system failures [5]. The poor seismic performance exhibited by these systems was mainly caused by inadequate bracing of the suspended pipes. Piping systems inadequately restrained may experience damage as a result of excessive displacements of the system or impact with other

* Corresponding author.
E-mail addresses: derek.rodriguez@iusspavia.it (D. Rodriguez), daniele.perrone@unisalento.it (D. Perrone), andre.filiatrault@iusspavia.it, af36@buffalo.edu (A. Filiatrault).
[1] Present affiliation: University at Buffalo, USA

https://doi.org/10.1016/j.engstruct.2025.120188
Received 4 August 2024; Received in revised form 27 November 2024; Accepted 17 March 2025
Available online 28 March 2025

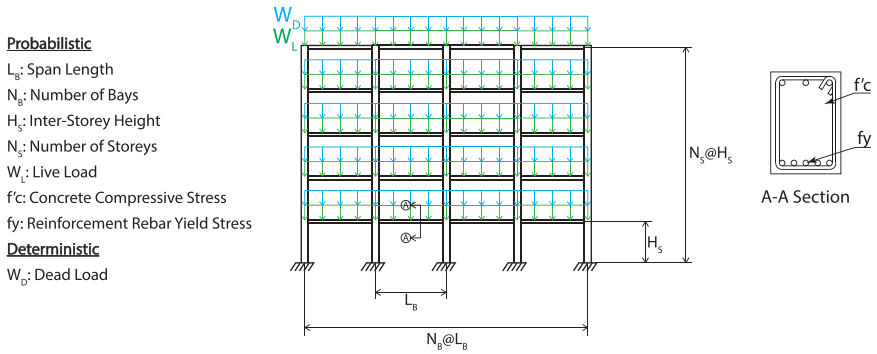

Fig. 1. Variables and geometry considered in the Monte Carlo simulation for the generation of the building portfolio by Perrone et al. [14].

adjacent structural members or NSEs.

Seismically designed suspended piping systems usually consists of the piping elements, hanger-rods or trapezes designed for gravity loads, and transverse and longitudinal sway-braced trapezes or rods that are meant to minimize the lateral swaying of the pipes and increase the lateral stiffness of the system. One recurrent issue with the seismic design and analysis of NSEs, and more specifically with suspended piping systems, is the lack of extensive experimental data and numerical studies, which hinders the understanding of the real response and performance of these systems when dynamically excited by a seismic event. In recent years, several investigations have been conducted to understand better how these systems respond during an earthquake. Perrone et al. [6] conducted an experimental campaign that tested four different suspended trapeze assemblies. Monotonic and reverse cyclic tests were conducted for all the specimens to determine suitable response parameters and engineering demand parameters (EDP) to establish performance objectives of suspended piping restraint installations. In order to increase the number of performance parameters currently available for suspended piping systems in the public literature, Perrone et al. [7] conducted a numerical study in which numerical models were developed based on component testing. Wood et al. [8] tested several connections and components of suspended trapeze assemblies under reverse cyclic loading to conduct numerical model calibration. Tian et al. [9] conducted an experimental campaign that tested 48 pressurized tee joint specimens of several diameters, materials and connection typologies through monotonic and reverse cyclic loading to determine rotational capacities at first leakage. Tian et al. [10] also conducted a numerical study in which numerical models were calibrated based on the data generated in the experimental campaign to predict the moment-rotation response of pressurized tee joints under dynamic loading. Finally, Blasi et al. [11] studied the effect of vertical floor accelerations in the seismic performance of suspended piping systems by conducting tri-directional non-linear time history analysis (NLTHA) of two different plan configurations of piping systems. It was found that for the studied archetypes, the vertical accelerations had a negligible effect on the damage rate of the suspended piping systems.

One common assumption that is used when analysing and designing suspended piping systems is that the lateral stiffness of the gravity load trapezes is negligible in comparison with that of the sway-braced trapezes. This assumption usually results in sway-braced trapezes being conservatively designed to sustain the totality of the seismic loading. One of the main reasons for implementing this approach, is the lack of experimental and numerical data on the seismic performance of gravity load trapezes, given that most of the studies currently available in the public literature focuses on the seismic performance of sway-braced trapezes [6,8]. Although it can be argued that the lateral stiffness of gravity load trapezes is expected to be lower than that of the sway-braced trapezes due to the lack of a lateral bracing element, the effect of considering a more realistic modelling approach for the gravity load trapezes in the overall seismic performance of suspended piping systems is unclear.

This paper presents the results of a parametric investigation to determine the influence of gravity load trapezes in the global seismic performance of suspended piping systems. Two different suspended piping layouts installed in four different reinforced concrete moment-resistant frames were designed according to Eurocode 8 [12] by varying the values of the behaviour factor (q_a). Numerical models of the resulting archetype designs were constructed in the open source platform OpenSees [13] considering two different conditions: i) neglecting lateral stiffness of the gravity load supports, and ii) assuming an elastic-perfectly plastic response of the gravity load trapezes (referred to from this point onwards as hangers) defined according to the material and section properties provided by the manufacturer technical specifications. Bi-directional (horizontal) NLTHA of the resulting suspended piping index archetypes was conducted by using floor motions obtained through a cascading analysis approach, by conducting NLTHAs of the reinforced concrete moment-resistant frames (MRFs) in which the suspended piping systems were to be installed using nine ground motion sets of increasing seismic hazard level (30, 50, 70, 100, 140, 200, 475, 975 and 2475-year return period). The obtained results are compared by means of fragility curves derived using two different limit states and recommendations are provided. Considering the potential contribution of the gravity load trapezes to the overall seismic performance of suspended piping systems could lead to more economical designs. Additionally, in the performance-based earthquake engineering framework, accurate estimation of engineering demand parameters (EDPs) is crucial to determine consistent and reliable decision variables (e.g., economic losses, downtime, casualties, etc.). The results from this study can contribute to improving the quantification of EDPs for suspended piping systems.

2. Determination of seismic demand

The seismic demand on NSEs is highly dependent on the dynamic properties of the supporting structures. To account for the dynamic filtering that the supporting structure produces in earthquake ground motions, a cascading analysis (i.e., decoupling the dynamic response of the NSE from that of the supporting structure) approach was adopted for this investigation. For the suspended piping index archetypes and target supporting structures considered in this investigation, the highest ratio of suspended piping system weight to total weight of the supporting structure and piping system is approximately equal to 0.5 %. Therefore, following the recommendations of the ASCE/SEI 7–22 [14], and Hadjian and Ellison [15], the influence of the dynamic response of the suspended piping index archetypes in the dynamic response of the supporting structure is neglected.

Four different reinforced concrete MRFs of varying fundamental periods were considered as the supporting structures in which the suspended piping systems were to be installed. These four MRFs were extracted from a population of 100 MRFs generated through a Monte

Table 1
Fundamental period and number of storeys of the selected reinforced concrete MRFs.

Building ID	T_1 *(s)*	N_S
1	0.52	4
2	1.04	6
3	0.43	3
4	0.30	2

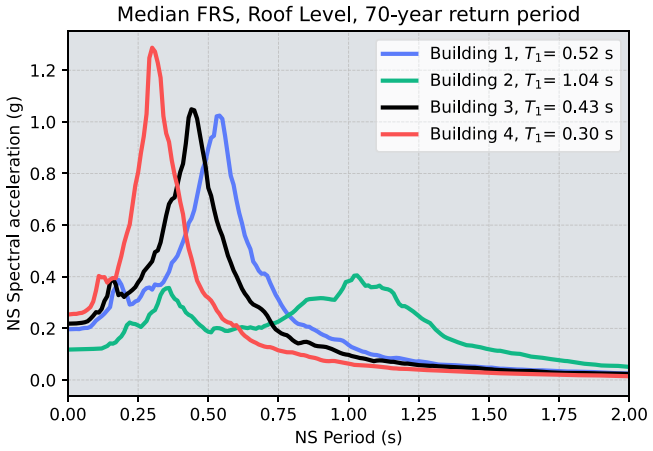

Fig. 2. Median FRS for all the considered supporting structures for a 70-year return period.

Carlo simulation by Perrone et al. [16]. These frames were designed according to Eurocode 8 seismic provisions assuming a force reduction factor $q = 3.75$, corresponding to a ductility class B, for a site close to the city of Cassino, Italy, characterized by a design peak ground acceleration of 0.21 g for a return period of 475 years. Fig. 1 shows a summary of the geometry, and the probabilistic and deterministic variables considered in the Monte Carlo simulation for the generation of the 100 reinforced concrete MRFs population, while Table 1 lists the fundamental periods and number of storeys of the four reinforced concrete MRFs selected for this investigation. Fig. 2 shows the median floor response spectrum (FRS) at the roof level of each selected supporting structure for a 70-year return period. The distinct spectral shapes exhibited by each supporting structure illustrate the influence that the dynamic properties of the selected supporting structures have on the amplitude and frequency content of the resulting floor motions.

Numerical models of the selected reinforced concrete MRFs were developed in the open-source platform OpenSees [13]. A fibre-based approach using inelastic beam-column fibre elements was used to model the MRFs structural elements including both material and geometric non-linearities. The uniaxial confinement model proposed by Priestley et al. [17] was used to simulate the cyclic response of concrete and a bilinear constitutive model with isotropic strain hardening equal to 1 % of the initial elastic modulus was implemented for the steel reinforcement. Finally, Rayleigh initial stiffness proportional viscous damping with 5 % critical damping specified in the first two elastic modes was considered in the numerical models to simulate the inherent damping of the structure. More details on the numerical modelling approach are reported in Perrone et al. [16].

To conduct the ground motion record selection, the seismic hazard characteristics and features of the European region, and more specifically Italy, were considered. According to the probabilistic seismic hazard assessment of Italy conducted by Stucchi et al. [18] and the seismic hazard maps provided by the Italian building code [19], the median peak ground acceleration (PGA) for the Italian territory is approximately equal to 0.14 g for a return period of 475 years, while the median plus one standard deviation PGA is close to 0.20 g. Based on this

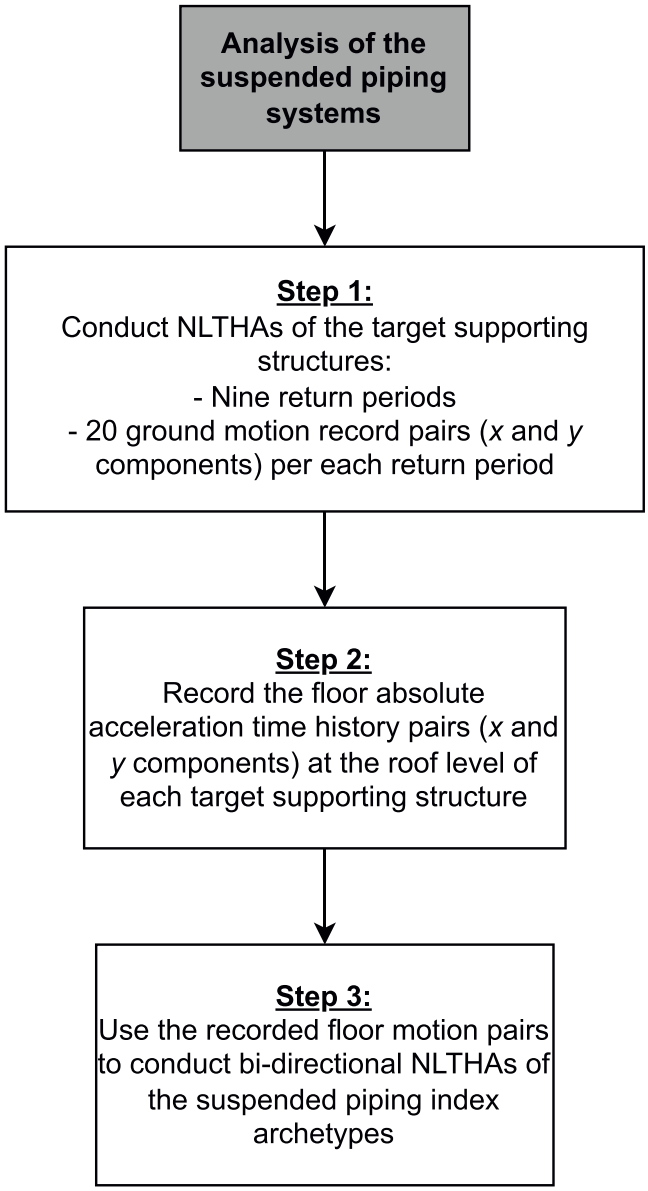

Fig. 3. Analysis procedure of the suspended piping index archetypes.

estimation, a site close to the city of Cassino, Italy, characterized by a PGA equal to 0.21 g for a return period of 475 years was selected. By comparing the seismic hazard of the selected site with European hazard maps [20], it was determined that the selected site can be considered representative, with reasonable approximation, of a medium-to-high seismicity far-field site for the entire European region. The record selection for the selected site was performed by considering nine return periods of the seismic hazard of increasing intensity (30, 50, 70, 100, 140, 200, 475, 975 and 2475-year return periods, respectively). For each return period, hazard-consistent selection of 20 horizontal ground acceleration orthogonal record pairs (i.e., two ground acceleration time-histories in the x and y orthogonal directions per record, respectively) was conducted from the PEER NGA-West database [21] based on spectral compatibility with a conditional mean spectrum according to the methodology proposed by Jayaram et al. [22]. The conditional periods used for the record selection were obtained by conducting eigenvalue analysis of the 100 reinforced concrete MRFs previously described in this section. Based on the obtained fundamental vibration period distribution, three different conditional periods equal to 0.3, 0.5 and 1.0 s were considered for the record selection. To conduct the analysis of

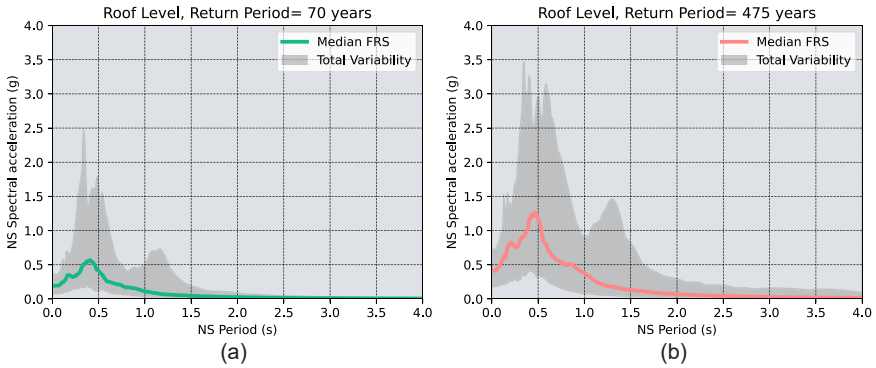

Fig. 4. Median floor response spectra and total variability at the roof level for two sample return periods: a) 70-year return period, and b) 475-year return period.

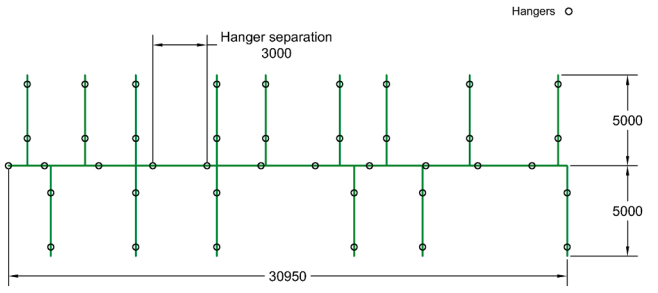

Fig. 5. Geometrical configuration of the suspended piping system with branches (units in millimeters).

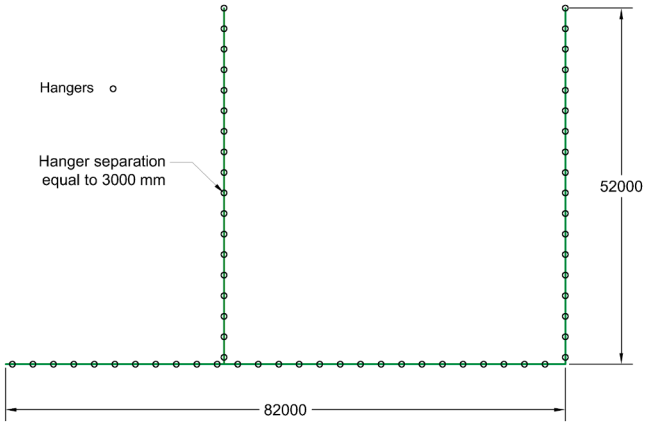

Fig. 6. Geometrical configuration of the suspended piping system without branches (units in millimeters).

a specific reinforced concrete MRF, the records sets selected for the conditional period that most closely matches the fundamental vibration period of the reinforced concrete MRF are used. The effect of the vertical component of the ground motions was not considered in this study, given that previous authors have found a negligible effect of vertical acceleration on the damage of suspended piping systems [11,23]. One of the main reasons for this behaviour, is the decoupling between the much higher frequency content of vertical floor motions compared to the flexural vibration frequencies of piping systems. Therefore, only horizontal components of the ground motions were selected to conduct the analyses of the suspended piping systems. More information on the ground motion record selection can be found in Perrone et al. [16] and O'Reilly et al. [1].

Once the ground motions and the numerical models of the selected MRFs were defined, NLTHAs were conducted to create an absolute floor acceleration time-history database to be used in the analysis of the suspended piping systems. Only roof-level absolute acceleration time-history pairs were recorded, given that floor spectral accelerations are expected to be higher near the roof-level of the supporting structures, therefore representing the most demanding condition for the seismic design of NSEs. This resulted in a final floor motion pair database consisting of 720 absolute floor acceleration time-history orthogonal pairs (4 buildings * 9 return periods * 20 ground motion orthogonal pairs= 720 floor motion orthogonal pairs). Fig. 3 shows a flowchart summarizing the steps followed to determine the floor motion pair database and conduct the NLTHAs of the selected suspended piping index archetypes in Section 5. Fig. 4 shows the roof level median floor response spectra (FRS) and total variability envelope for two sample return periods (70 and 475-year return periods, respectively) of the selected buildings for one of the horizontal components of the selected ground motions. The total variability is defined as the sum of the record-to-record and building-to-building variabilities.

Table 2
Definition of suspended piping index archetypes.

	Key Archetype Design Parameters					
Archetype ID	***Geometry***	***Pipe Material***	***Pipe Diameter (mm)***	***Pipe Ring Typology***	q_a	T_a/T_1
1	WB	Steel	127	Stiff Pipe Ring	1	1
2	WB	Steel	127	Stiff Pipe Ring	2	1
3	WB	Steel	127	Stiff Pipe Ring	3	1
4	WB	Steel	127	Stiff Pipe Ring	4	1
5	WOB	Steel	127	Stiff Pipe Ring	1	1
6	WOB	Steel	127	Stiff Pipe Ring	2	1
7	WOB	Steel	127	Stiff Pipe Ring	3	1
8	WOB	Steel	127	Stiff Pipe Ring	4	1

3. Design of the non-structural index archetypes

The design provisions of Eurocode 8 [12] were used for the design of the selected suspended piping index archetypes. As it was discussed in Section 2, roof-level seismic demand is considered for the analysis of the suspended piping index archetypes, given that it produces the most demanding scenario in terms of location within a supporting structure dominated by its first mode response. In this context it is important to clarify that additional prescriptive design requirements that are usually implemented for suspended piping restraint installations in other design

Table 3
Theoretical spacing and number of sway-braced trapezes for each archetype design.

		Theoretical spacing (m)		*Number of sway braced trapezes*	
Archetype ID	***Layout section***	***Transverse***	***Longitudinal***	***Transverse***	***Longitudinal***
1	Main line	3	7	10	5
	Branch line			2	1
2	Main line	6	15	5	3
	Branch line			1	1
3	Main line	9	22	4	2
	Branch line			1	1
4	Main line	13	30	3	2
	Branch line			1	1
5	Main line	3	7	25	11
	Cross main line			16	7
6	Main line	6	15	13	6
	Cross main line			8	4
7	Main line	9	22	9	4
	Cross main line			6	3
8	Main line	13	30	7	3
	Cross main line			4	2

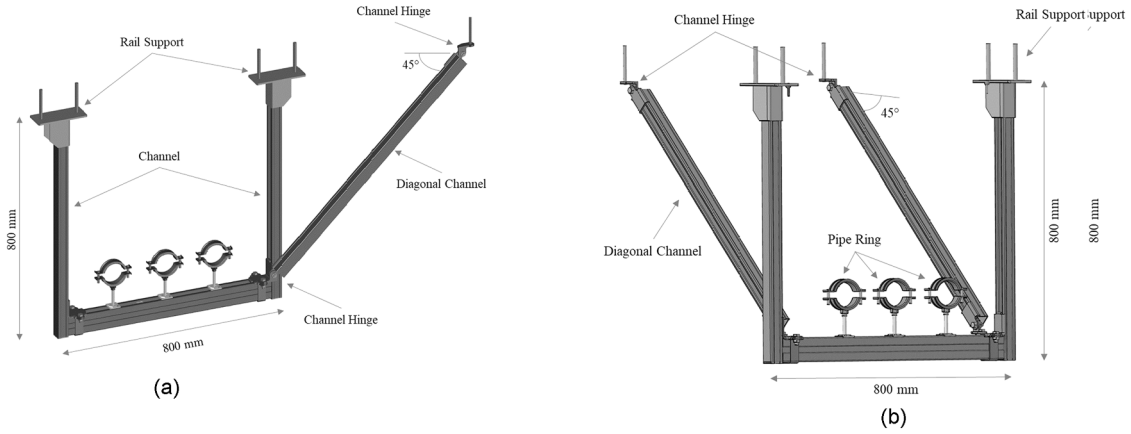

Fig. 7. a) Transverse and b) Longitudinal sway-braced trapezes.

standards, such as the ones included in the NFPA13 standard [24], will not be considered. The static horizontal design force, F_a, is defined as follows:

$$F_a = \frac{S_a W_a \gamma_a}{q_a} \tag{1}$$

where W_a is the seismic weight of the NSE, γ_a is the importance factor, q_a is the behaviour factor to be calibrated, and S_a is the seismic coefficient applicable to NSEs, defined as:

$$S_a = \alpha S \left[3 \frac{\left(1 + \frac{z}{H}\right)}{\left(1 + \left(1 - \frac{T_a}{T_1}\right)^2\right)} - 0.5 \right] \tag{2}$$

where α is the ratio of the design ground acceleration (475-year return period) on type A ground, to the acceleration of gravity g, S is the soil factor, T_a is the fundamental vibration period of the NSE, T_1 is the fundamental vibration period of the supporting structure, z is the height of the NSE above the level of application of the seismic action, and H is the building height measured from the foundation or from the top of a rigid basement.

It is worth noting that Eurocode 8 does not provide equations to estimate the fundamental vibration period of the NSE (T_a). Additionally, in most cases practitioners do not have available the required data to construct a reliable numerical model of the target NSE. As a result, two limiting conditions are considered in practice to implement Eq. (2): i) Assuming a T_a/T_1 ratio equal to unity, which corresponds to the case in which the fundamental vibration mode of the NSE is in resonance with the fundamental vibration mode of the supporting structure, and ii) assuming a T_a/T_1 ratio equal to zero, which corresponds to the case in which the NSE is considered rigid, therefore no amplification of the floor acceleration demand is expected in the NSE.

In equivalent static design procedures, a satisfactory seismic design is achieved when the horizontal design seismic force is equal or less then the characteristic strength (F_{Rk}) of the non-structural seismic force-resisting system (SFRS) reduced by a resistance factor (γ_m):

$$F_a \leq \frac{F_{Rk}}{\gamma_m} \tag{3}$$

In the case of suspended piping restraint installations, the operating weight of the system can be calculated as follows:

$$W_a = 1.15 N_p w_a s_a \tag{4}$$

where N_p is the number of pipes supported by each sway-braced trapeze, w_a is the unit weight of water filled pipes, s_a is the spacing of the sway-braced trapezes and the 1.15 factor considers the supplemental weight of the fittings and welded connections [21].

By combining Eqs. (1), (3) and (4) the required spacing of the sway-braced trapezes (s_a) can be calculated as follows:

$$s_a \leq \frac{F_{Rk} q_a}{1.15 \gamma_m \gamma_a S_a w_a N_p} \tag{5}$$

The designs of the archetype are conducted by calculating the

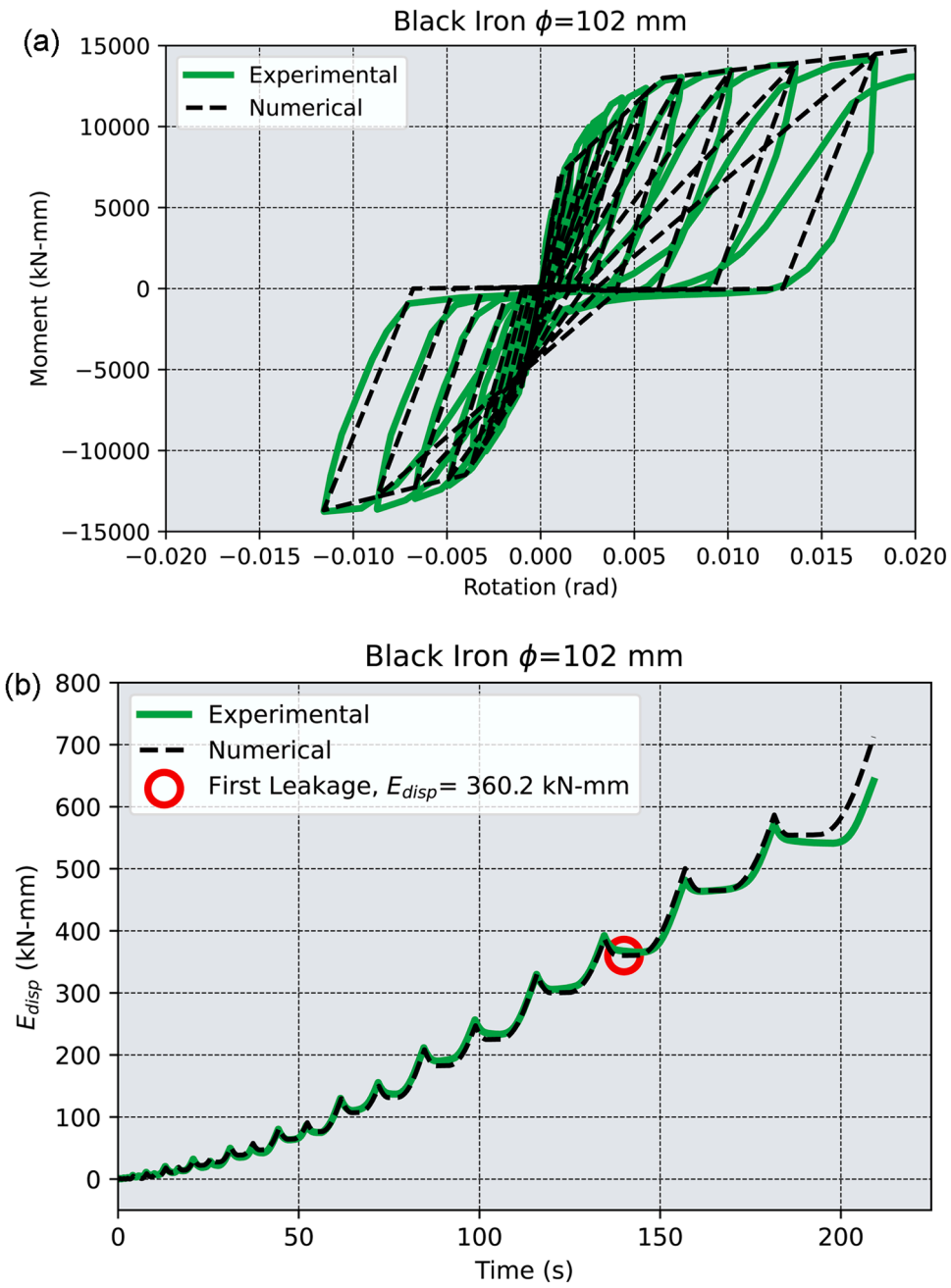

Fig. 8. Calibration of the Hysteretic material model for the 102 mm-diameter steel threaded joint: a) Moment-rotation hysteretic response, and b) Dissipated energy time-history.

required spacing s_a to fulfil an initial assumption for the value of q_a.

To reproduce the seismic response of the suspended piping restraint installations, the results of the experimental campaign conducted by Perrone et al. [6], and the numerical models developed in Perrone et al. [7] were used. To model the seismic response of the piping joints, the experimental program conducted by Tian et al. [9], and the numerical models developed by Tian et al. [10] were selected.

Mechanical piping plan distributions are typically driven by the use and layout of the building in which they will be installed. Based on a survey conducted for real construction projects, it was determined that two types of plan distributions can be generally found for suspended piping systems: i) plan distributions with branches (WB), which can be typically found in buildings with corridors and equally divided spaces, as for example residential or office buildings, and ii) plan distributions without branches (WOB), which are typically found in buildings with large open spaces, as for example warehouses and industrial facilities. For the definition of the suspended piping index archetype designs, the plan distributions shown in Fig. 5 and Fig. 6 are used, which are meant to describe both types of layouts. The layout with branches (Fig. 5) consists of a main line 31-m long, with 15 perpendicular 5-m long branch lines. On the other hand, the layout without branches (Fig. 6) consists of one 82-m long main line with two perpendicular 52-m long cross main lines.

The material and number of pipes influence the global response of the suspended piping system since they affect the seismic mass, the stiffness of the suspended pipes and the gravity loads resisted by the hangers and the sway-braced trapezes. For this investigation, a configuration consisting of three separate steel pipes with threaded joints with a diameter equal to 127 mm (5 in) is considered. To determine the hanger separation, the pipe characteristics and operation gravity loads

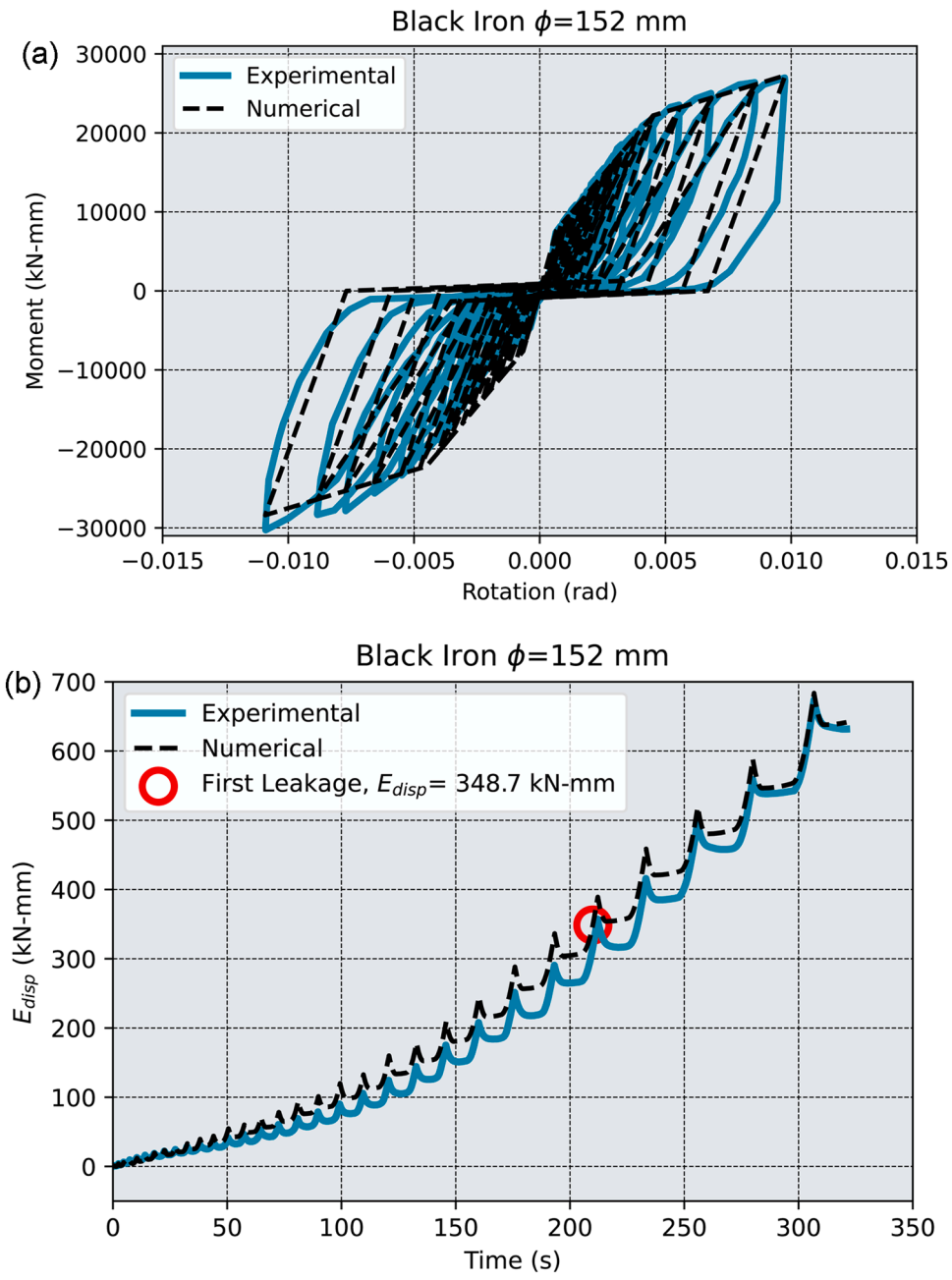

Fig. 9. Calibration of the Hysteretic material model for the 152 mm-diameter steel threaded joint: a) Moment-rotation hysteretic response, and b) Dissipated energy time-history.

should be considered. Additionally, maximum spacing specified by the manufacturer and/or applicable design requirements should also be taken into account. In this study, the pipes are considered filled with water, and the hanger separation is set equal to 3 m based on the pipe material (steel pipes) and following the recommendations of the manufacturers (based on gravity load analysis) during other collaborative studies [6,25]. Finally, stiff pipe rings, in which the steel pipes are in direct contact with the pipe rings are considered.

The index archetype designs are conducted by implementing Eq. (5) for various assumed values of the q_a factor and assuming a value of the T_a/T_1 ratio equal to unity, which corresponds to the most demanding design condition in which the fundamental mode of the NSE is in resonance with that of the supporting structure. Trial values of the q_a factor equal to 1, 2, 3 and 4 were assumed. The final outcome is a total of eight archetype designs, which are described in Table 2, while a summary of the theoretical spacing obtained by means of Eq. (5) is shown in Table 3. In Table 3, the resulting number of sway-braced trapezes is also shown for each of the layout sections of the each archetype. With regards to the piping joints, two different criteria were considered for defining their locations: i) every 6 m in straight pipe sections, since this is typically the standard maximum length of fabrication for most piping systems, and ii) at 100 mm before and after every intersection of steel pipes, since the typical length of steel piping joints is 200 mm.

4. Non-linear models development

Based on the archetype designs conducted in Section 3, three-dimensional numerical models of each archetype were constructed with the open-source platform OpenSees [13]. Since in several studies [6,9,26–29] it has been found that the non-linear behaviour of

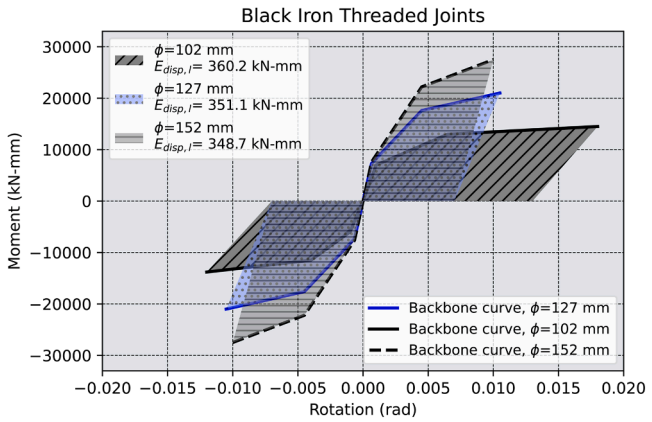

Fig. 10. Illustration of the calibration process of the hysteretic parameters for the 127 mm diameter steel threaded joint.

Table 4
Calibrated parameters of the Hysteretic material model from the OpenSees material library for 102, 127, and 152 mm diameter piping joints.

Parameter	*102 mm-diameter*	*127 mm-diameter*	*152 mm-diameter*
s1p (kN*mm)	7.00E+ 03	7.30E+ 03	7.60E+ 03
e1p (rad)	1.00E−03	6.50E−04	6.50E−04
s2p (kN*mm)	1.30E+ 04	1.76E+ 04	2.22E+ 04
e2p (rad)	6.50E−03	4.70E−03	4.50E−03
s3p (kN*mm)	1.45E+ 04	2.10E+ 04	2.75E+ 04
e3p (rad)	1.80E−02	1.10E−02	1.00E−02
s1n (kN*mm)	−6.00E+ 03	−7.30E+ 03	−7.60E+ 03
e1n (rad)	−1.00E−03	−6.50E−04	−6.50E−04
s2n (kN*mm)	−1.15E+ 04	−1.76E+ 04	−2.22E+ 04
e2n (rad)	−4.00E−03	−4.70E−03	−4.50E−03
s3n (kN*mm)	−1.38E+ 04	−2.10E+ 04	−2.75E+ 04
e3n (rad)	−1.20E−02	−1.10E−02	−1.00E−02
pinchx	5.00E−01	8.50E−01	8.00E−01
pinchy	1.00E−02	5.00E−02	5.00E−02
damage1	0.00E+ 00	0.00E+ 00	0.00E+ 00
damage2	0.00E+ 00	0.00E+ 00	0.00E+ 00
beta	3.00E−01	1.00E−01	1.00E−01

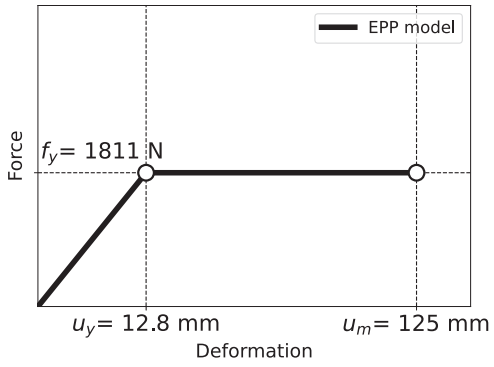

Fig. 11. Definition of the EPP model for suspended piping hangers, where f_y is the yield lateral force of the hanger, u_y is the corresponding yield lateral deformation of the hanger, and u_m is the ultimate lateral deformation of the hanger.

suspended piping systems concentrate in the pipe joints and connections to the supporting structure, all the pipes were modelled as elastic beam elements suspended 800 mm from the roof level slab of the characteristic buildings, as shown in Fig. 7. All the nodes of the model were free to deform in the translational and rotational degrees-of-freedom except for the nodes at the location of the static supports, in which the vertical translation was restrained. The transverse and longitudinal sway-braced

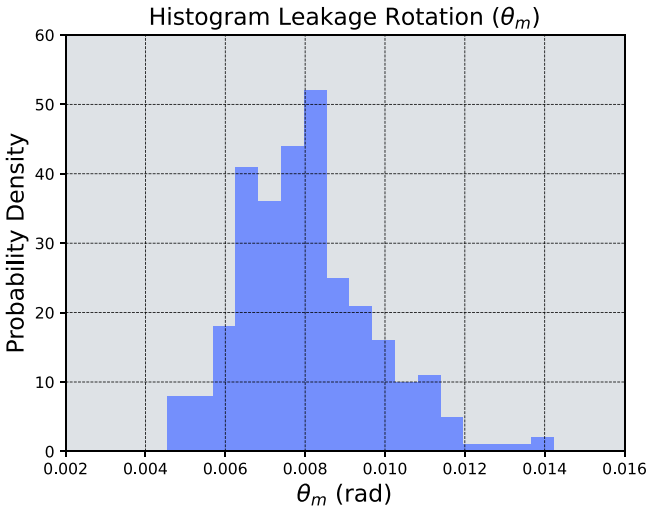

Fig. 12. Histogram of a random sample of the leakage rotation (θ_m) assuming a sample size equal to 300 using the lognormal distribution parameters proposed by Tian et al. [9].

Table 5
Performance parameters of the sway-braced trapezes.

Sway braced trapezes performance parameters				
Bracing Orientation	**Δ_y (mm)**	**Δ_u *(mm)***	μ_{1T}	μ_{2T}
Transverse	20.11	47.91	1.00	2.40
Longitudinal	34.00	80.00	1.00	2.40

trapezes were modelled by using non-linear springs calibrated with the hysteretic response of the trapezes by using the "Pinching4" material from the OpenSees material library. The experimental data generated by Perrone et al. [6], and the numerical models developed in Perrone et al. [7] were used to perform the calibration of the hysteretic response of the trapezes. For the piping joints, the experimental data generated by Tian et al. [9], and the numerical models developed in Tian et al. [10] were used to define non-linear rotational springs that recreate the response of the steel piping threaded joints. Since Tian et al. [10] calibrated the Hysteretic material model from the OpenSees material library only for the 50 mm-diameter steel threaded joints, the experimental results from Tian et al. [9] were used to calibrate the hysteretic material model for the 102 and 152 mm-diameter steel threaded joints based on their hysteretic response and dissipated energy time-histories. Using the calibrated hysteretic curves (shown in Fig. 8a and Fig. 9a), the total dissipated energy at first leakage ($E_{disp,l}$) was calculated. Fig. 8b and Fig. 9b show the dissipated energy time-histories for the 102 and 152 mm-diameters threaded piping joints. In the same figures, the point at which the first leakage occurred is shown. As it is shown, the total dissipated energy at first leakage remains fairly constant for the two diameters (102 and 152 mm). Since 127 mm-diameter steel threaded joints were not tested in the experimental campaign conducted by Tian et al. [9], the hysteretic parameters for the 127mm-diameter steel threaded joint were obtained as follows:

- The median rotations at first leakage, and the moment capacities of the backbone curve were interpolated from those experimentally calibrated for the 102 and 152 mm-diameter steel threaded joints, following the trend reported by Tian et al. [9] for all the tested diameters.
- The rotation capacities of the backbone curve, and the shape of the hysteresis loops were calibrated so that the total dissipated energy at first leakage was equal to that of the 102 and 152 mm-diameters steel threaded joints (as it was explained in the previous paragraph, the total dissipated energy at first leakage for the 102 and 152 mm-

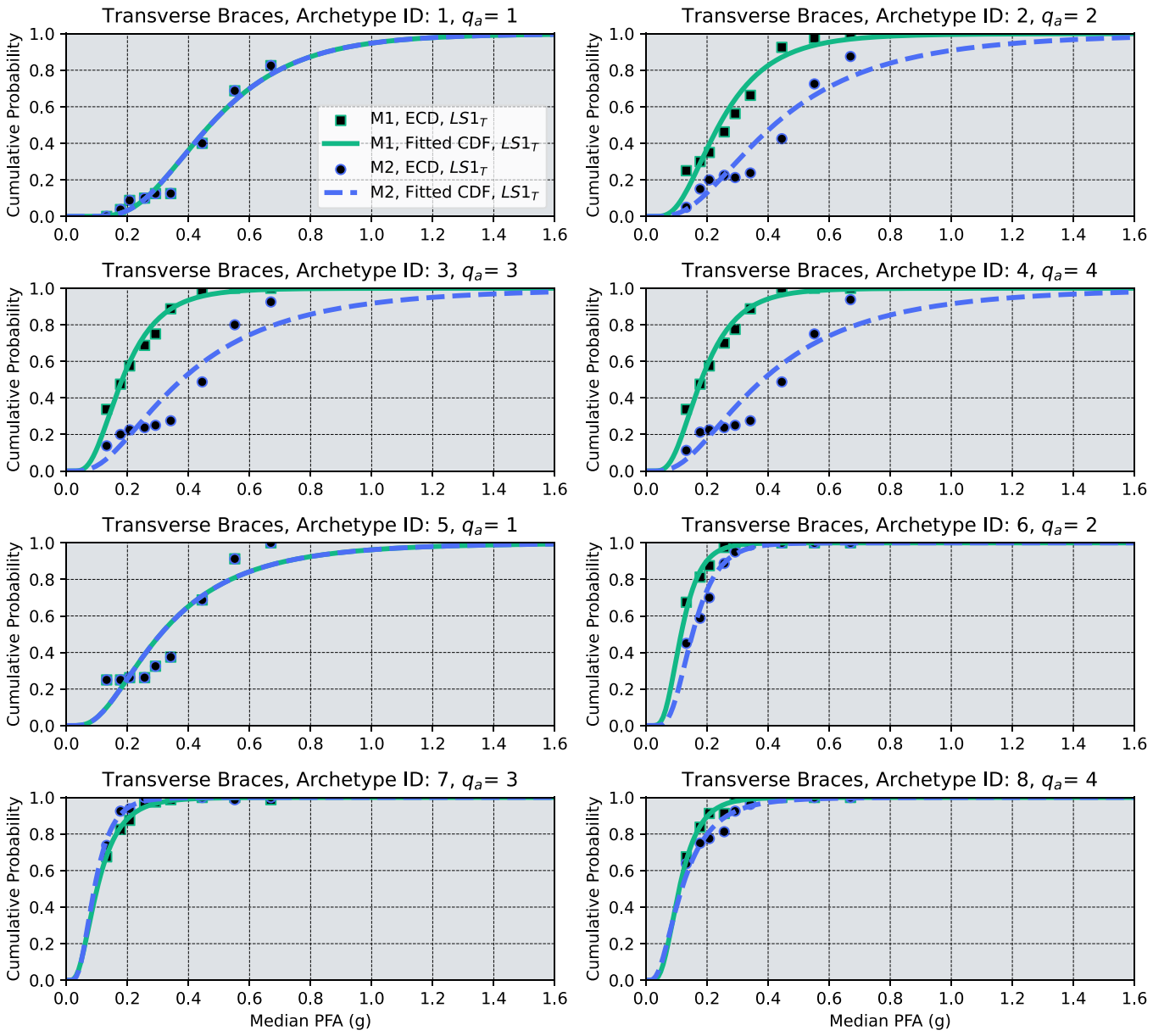

Fig. 13. Empirical cumulative distributions and fitted lognormal fragility curves for $LS1_T$ of transverse sway-braced trapezes and the two modelling approaches (M1 and M2).

diameter steel threaded joints remained fairly constant). For the calibration of the rotation capacities, only values equal or greater than that of the 152 mm-diameter steel threaded joint were considered, so that the observed tendency in the experimental tests conducted by Tian et al. was preserved (rotations capacities decrease as the diameter increases).

The process to obtain the hysteretic parameters for the 127 mm-diameter steel threaded joint described above is illustrated in Fig. 10. The calibrated parameters of the Hysteretic material model are shown in Table 4 for the 102, 127, and 152 mm-diameter steel threaded joints.

To determine the influence of the modelling approach of the hanger in the overall seismic performance of the suspended piping index archetypes, two different approaches were considered for modelling the hangers:

- Assuming a negligible lateral stiffness (referred to from this point onwards as M1). This was achieved by using elastic springs with a negligible stiffness in the locations of the hangers, so that the suspended piping displacements are not restricted at these locations.
- Considering explicitly the lateral behaviour of the hangers (referred from this point onwards as M2). This was achieved by using elastic-perfectly plastic (EPP) springs with an initial stiffness calculated according to the manufacturer technical specifications [30], and setting the maximum lateral displacement of the hangers equal to the ultimate displacement reported by Wood et al. [8] for longitudinally braced trapeze assemblies tested under monotonic loading in the transversal direction. Fig. 11 shows an illustration of the EPP model considered for the suspended piping hangers including the values of all the relevant parameters.

In this regard, it is worth mentioning that the orientation of the rail supports (Fig. 7) may play an important role in the seismic response of the hangers. The orientation of the rail supports often depends on project-specific characteristics and the engineering judgment of the designer [31]. The orientation of the rail supports of the hangers

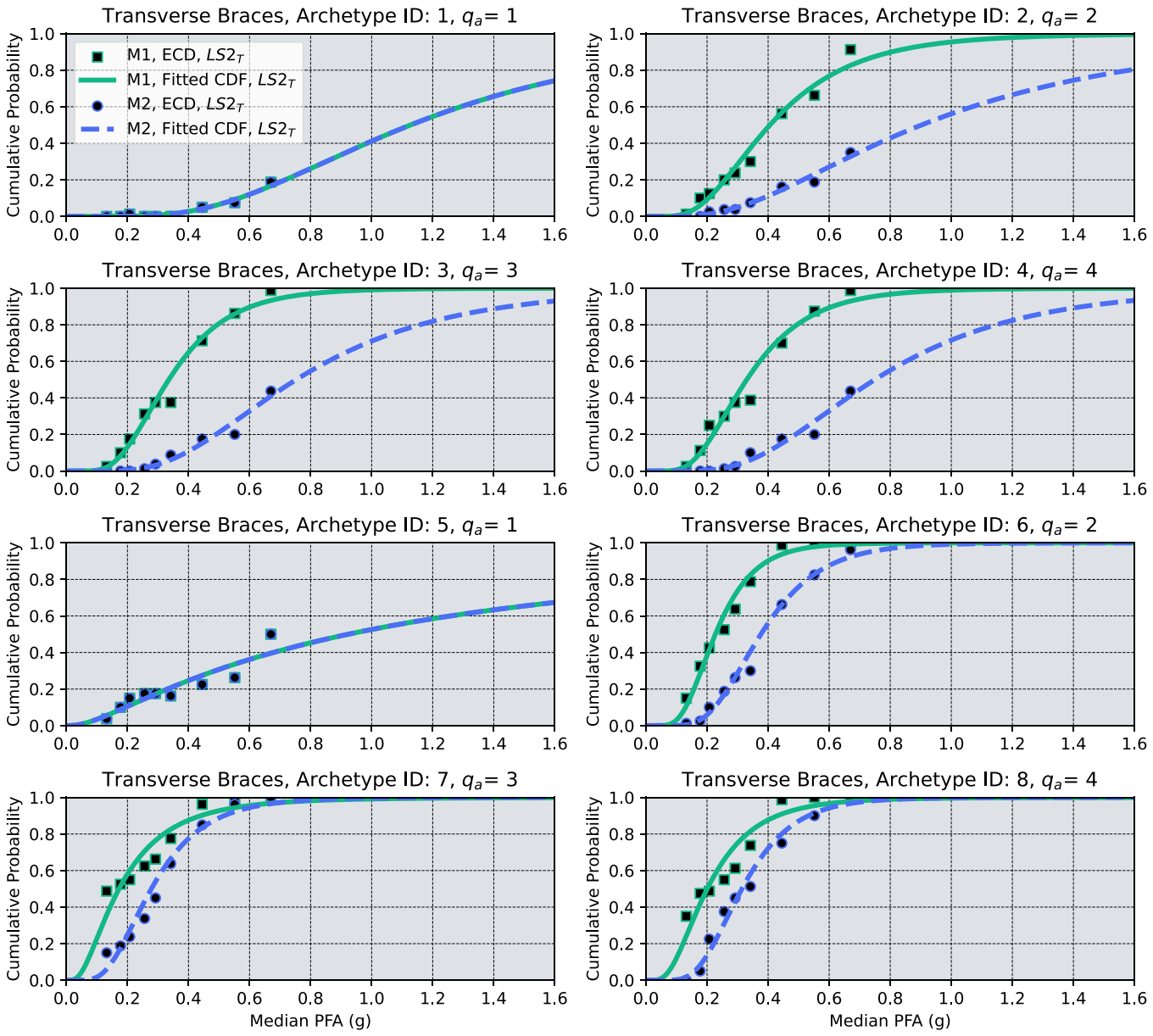

Fig. 14. Empirical cumulative distributions and fitted lognormal fragility curves for $LS2_T$ of transverse sway-braced trapezes and the two modelling approaches (M1 and M2).

influences the lateral stiffness of the hanger. In the longitudinal direction, the rail supports provide moment capacity, since they have at least two anchors aligned within the same axis, therefore under lateral loads one anchor is capable of sustaining tension forces, while the other sustains compression forces. In the perpendicular direction, the rail supports behaves closer to a pinned support, therefore no significant moment capacity is provided since the two anchors would likely sustain tension forces simultaneously. Since the criteria to define the orientation of the rail supports depend on conditions that are outside of the scope of this paper, the authors decided to assume the orientation of the rails supports aligned with the transversal direction of the suspended piping system. Finally, since the considered numerical models simulate explicitly the main source of energy dissipation of the suspended piping index archetypes, Rayleigh damping using a small damping ratio equal to 1 % of critical was applied to the first and third modes of the suspended piping system to account for additional sources of damping other than the hysteretic energy dissipation.

5. Non-linear analysis

Given that suspended piping systems can be installed along any of the two principal directions of a building, the ensemble of 720 floor accelerogram pairs were rotated 90 degrees to account for the different possible orientations of the suspended piping system within the supporting structure, resulting in a final collection of 1440 floor accelerogram pairs. Using this ensemble of floor accelerogram pairs, bidirectional NLTHAs were carried out following a multiple-stripe approach.

For the sway-braced trapezes, the results of the analysis are expressed in terms of fragility curves derived using the displacement ductility demand (μ_Δ) and the median PFA for each seismic hazard return period as the engineering demand parameter (EDP) and the intensity measure (IM), respectively. Fragility curves were derived separately for the two types of sway-braced trapezes considered. For the piping joints, the results are expressed in terms of fragility curves derived using the leakage rotation ratio (R_L) and the median PFA for

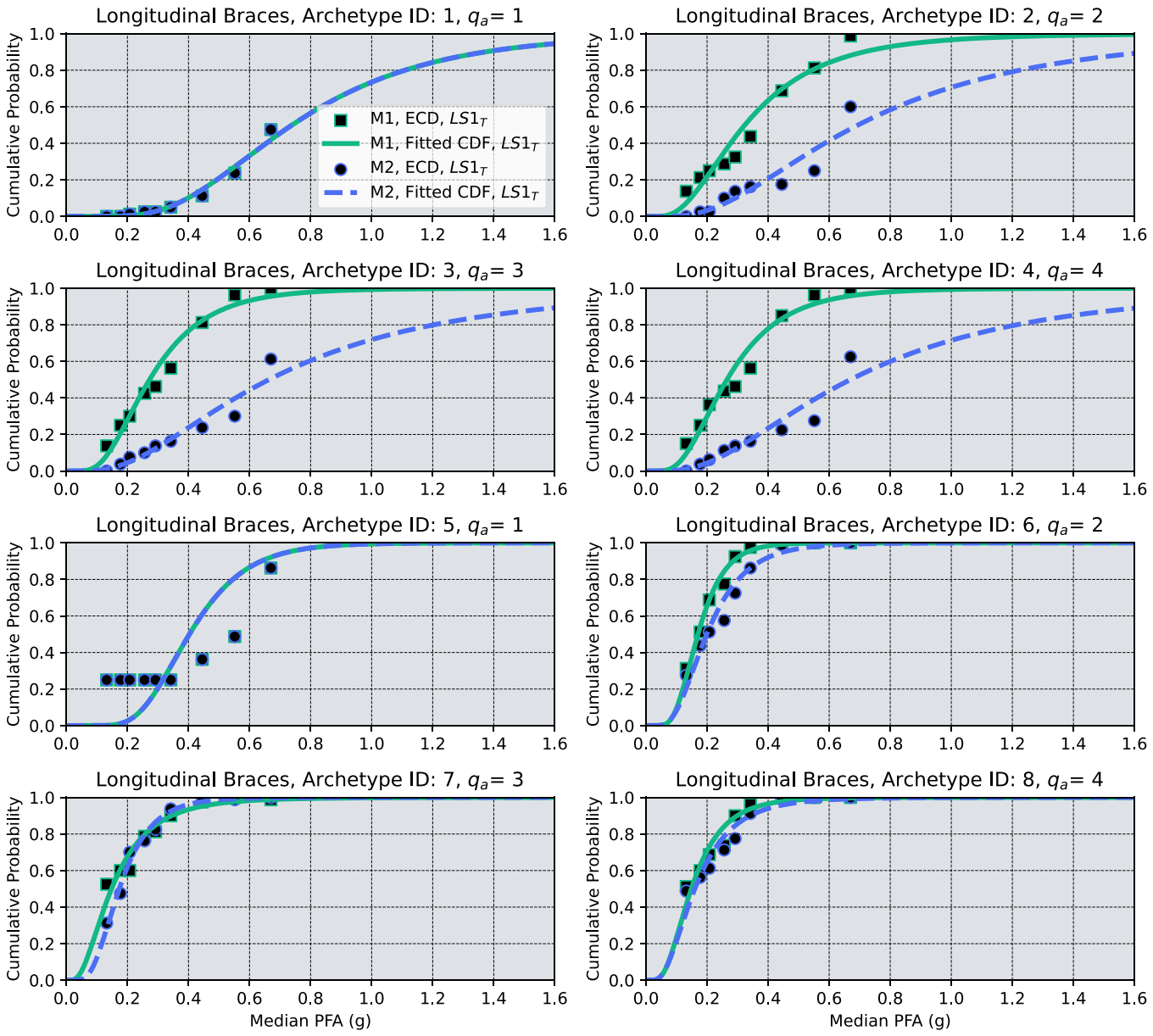

Fig. 15. Empirical cumulative distributions and fitted lognormal fragility curves for $LS1_T$ of longitudinal sway-braced trapezes and the two modelling approaches (M1 and M2).

each seismic hazard return period as the EDP and the IM, respectively. In the case of the sway-braced trapezes, the displacement ductility demand was defined as the ratio between the maximum relative displacement recorded at each analysis across all the sway-braced trapezes and the yield displacement, defined according to Perrone et al. [6] and Perrone et al. [7]. For the case of the piping joints, on the other hand, the leakage rotation ratio was defined as the maximum ratio between the maximum resultant rotation recorded at each piping joint of each analysis, and a random realization of the leakage rotation, which was defined as a random variable following a lognormal distribution as proposed by Tian et al. [9]. More specifically, for each piping joint, the leakage rotation was determined by assuming a lognormal distribution with parameters equal to the ones proposed by Tian et al. [9], and generating a random realization accordingly. Fig. 12 shows the histogram of a random sample of the leakage rotation (θ_m) assuming a sample size equal to 300 using the lognormal distribution parameters proposed by Tian et al. [9]. A lognormal distribution was considered for the derivation of the fragility curves by fitting the corresponding CDF to the empirical cumulative distributions (ECDs) following the recommendations provided by Baker [32] for multiple-stripe analysis. For the sway-braced trapezes, two limit states were established to derive the fragility curves and conduct the performance evaluation:

- The sway-braced trapezes remaining elastic, which translates into a displacement ductility demand equal to unity (referred to as $LS1_T$).
- The sway-braced trapezes experiencing damage but without compromising their capacity to sustain the gravity loads, which translates into a displacement ductility demand equal to the ultimate ductility demand obtained from the test results reported by Perrone et al. [6] (referred to as $LS2_T$).

For the case of the piping joints, only one limit state was considered, which was the occurrence of leakage through the piping joints, which translates into a leakage rotation ratio equal to unity (referred to as $LS1_{PJ}$). The parameters used to define the two selected limit states for the sway-braced trapezes are listed in Table 5, where Δ_y is the yield

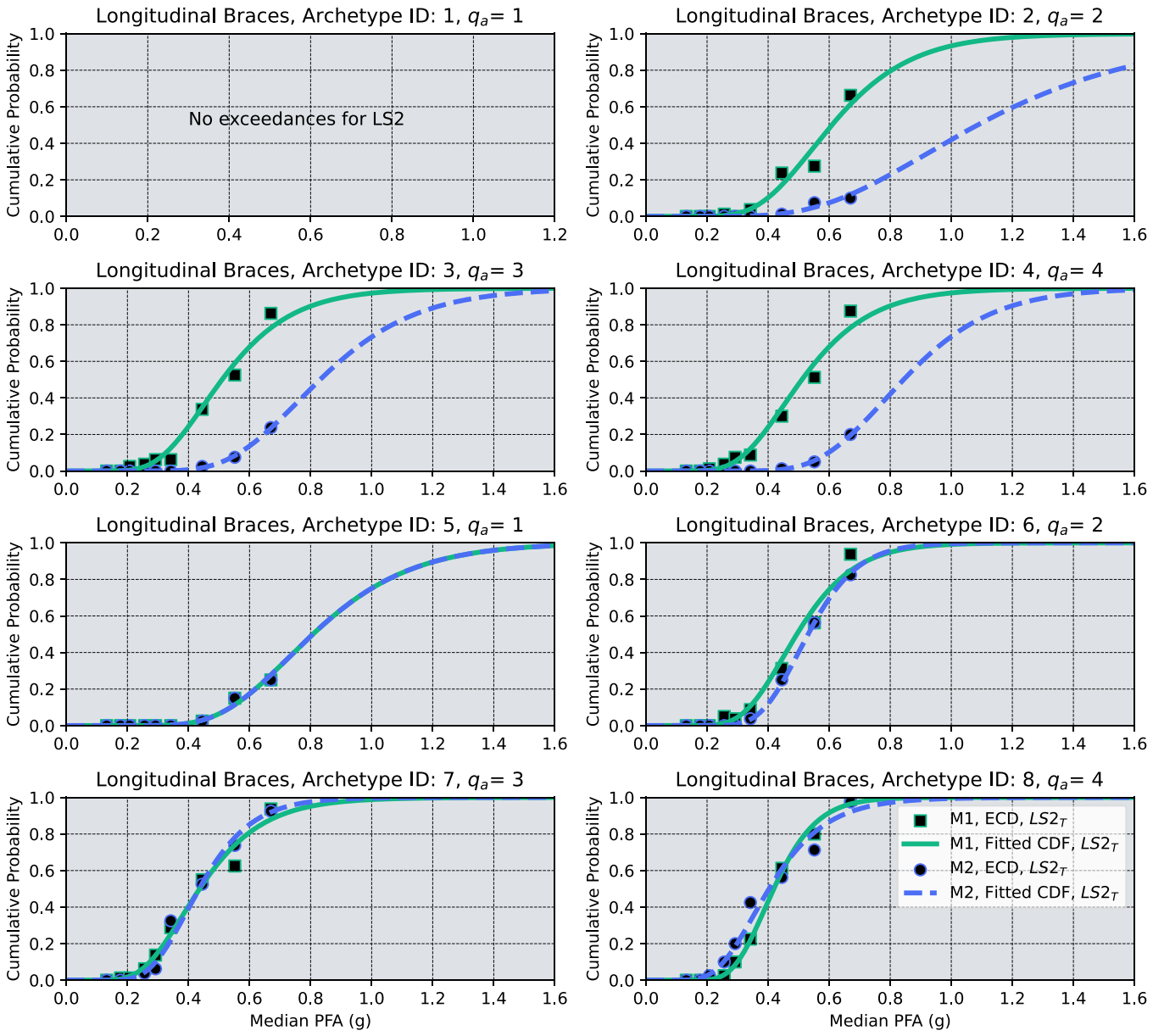

Fig. 16. Empirical cumulative distributions and fitted lognormal fragility curves for $LS2_T$ of longitudinal sway-braced trapezes and the two modelling approaches (M1 and M2).

displacement, Δ_u is the ultimate displacement, μ_{1T} is the target displacement ductility demand for $LS1_T$, and μ_{2T} is the target displacement ductility demand for $LS2_T$. As mentioned previously, the performance parameters shown in Table 5 were obtained from the experimental campaign conducted by Perrone et al. [6], in which monotonic and reverse cyclic tests of several sway-braced trapezes were conducted to evaluate different response parameters. Finally, since two sets of 720 accelerogram pairs were considered for the analyses (by rotating 90 degrees the original set of 720 accelerogram pairs obtained in Section 2), the EDPs were defined as the maximum values obtained from the NLTHAs conducted for the two orthogonal combinations for each of the 720 floor accelerogram pairs.

Fig. 13 and Fig. 14 show the ECDs and the fitted lognormal CDFs for the transverse sway-braced trapezes for $LS1_T$ and $LS2_T$, respectively. On the other hand, Fig. 15 and Fig. 16 show the ECDs and the fitted lognormal CDFs for the longitudinal sway-braced trapezes for $LS1_T$ and $LS2_T$, respectively. Finally, Fig. 17 shows the ECDs and fitted lognormal CDFs for the piping joints for $LS1_{PJ}$. The values of the lognormal distribution parameters obtained from the fitting process are shown in Table 6 for the transverse and longitudinal sway-braced trapezes, while the parameters obtained for the piping joints are shown in Table 7. The parameters presented in these tables correspond to the median of the fragility functions (θ) and the standard deviation of the natural logarithm of the IM (β). The acronym "N.E." stands for "No Exceedances".

As it is shown in Fig. 13 and Fig. 14, considering the EPP model of the hangers has a profound influence on the fragility curves of the transverse sway-braced trapezes for the two considered limits states. For values of the behaviour factor q_a larger than unity, a shift of the fragility curves towards higher values of PFA is observed. This shift is more pronounced for the suspended piping layouts with branches (Archetype IDs 1, 2, 3 and 4), and for the $LS2_T$ limit state. The suspended piping index archetypes that exhibited a larger shift in the fragility curves due to the implementation of the EPP modelling approach were the suspended piping index archetypes with branches. The main reason for this behaviour is that the fundamental vibration period of the suspended piping index archetypes with branches shortened more than in the

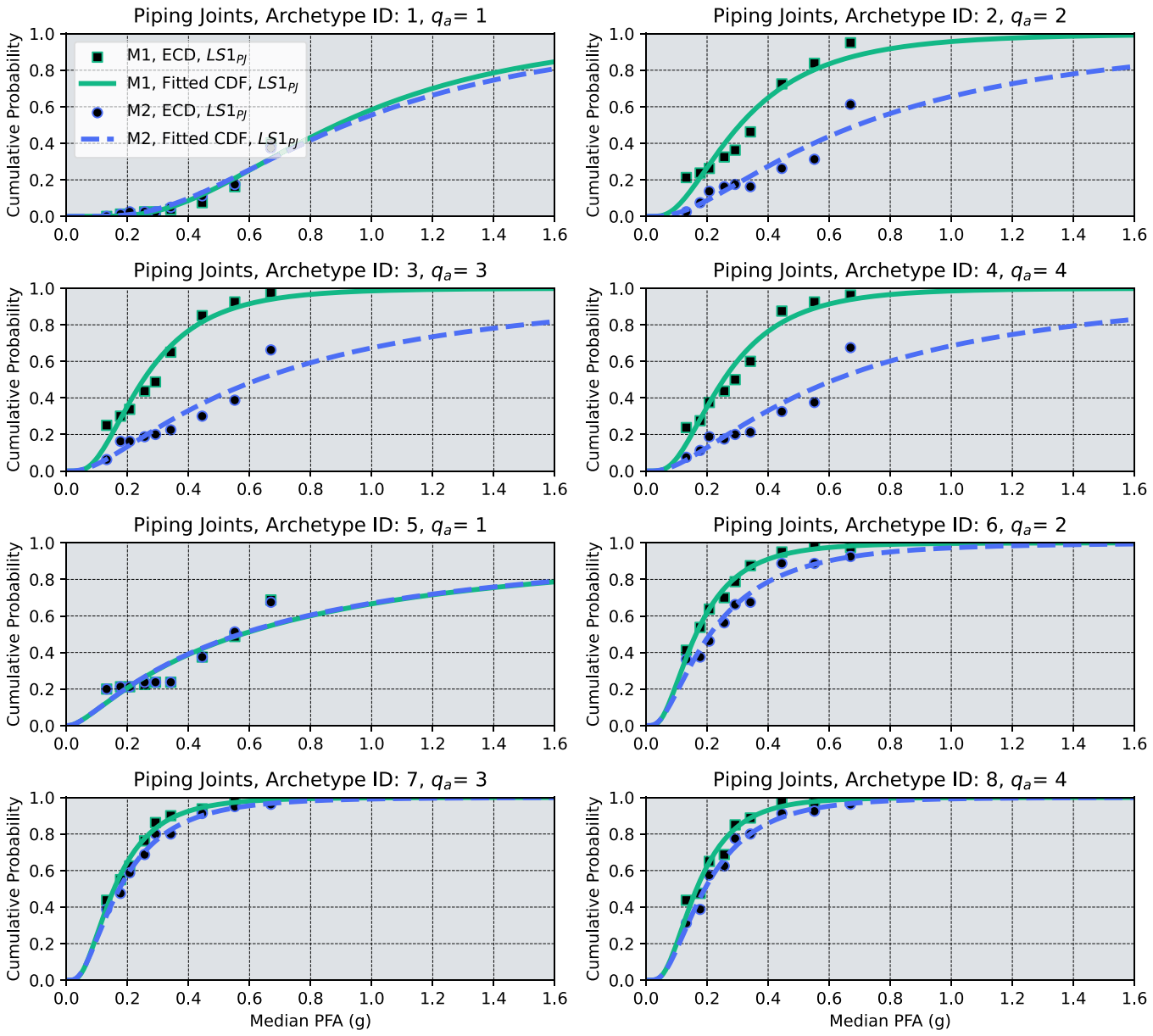

Fig. 17. Empirical cumulative distributions and fitted lognormal fragility curves for $LS1_{PJ}$ of the piping joints of the suspended piping system and the two modelling approaches (M1 and M2).

suspended piping index without branches when the EPP modelling approach was implemented. The more pronounced reduction of the fundamental vibration period observed for the suspended piping index archetypes with branches is explained by the fact that the hangers installed in the branches provide additional stiffness to the overall suspended piping system in the longitudinal direction, which does not happen in the same degree in suspended piping systems without branches. Table 8 shows a comparison of the fundamental vibration periods (T_{1SP}) of the suspended piping index archetypes considering the two modelling approaches (M1 and M2).

For of the longitudinal sway-braced trapezes, a similar trend to that of the transverse sway-braced trapezes occurs, as shown in Fig. 15 and Fig. 16. By comparing the fragility curves of the transverse and longitudinal sway-braced trapezes, it can be noted that the transverse sway-braced trapezes dominate the response of the suspended piping systems, given that the two proposed limits states are reached at lower levels of PFA for the transverse sway-braced trapezes than for the longitudinal sway-braced trapezes. In the case of the suspended piping system piping joints, the fragility curves derived using the leakage occurrence limit state also show a drift toward higher values of PFA when the EPP model is implemented in the modelling of the hangers, as it is shown in Fig. 17. As in the case of the fragility curves for the transverse and longitudinal sway-braced trapezes, the shift of the piping joints fragility curves is more pronounced for the suspended piping archetypes with branches.

The piping joints play an important role in the overall seismic performance of the suspended piping systems. Even if the seismic force-resisting system of the suspended piping performs adequately, if leakage through the piping joints takes place, the overall performance of the suspended piping system, and even of the supporting structure could be compromised. To determine if the performance of the piping joints or the trapezes dominates the overall seismic performance of the suspended piping system, the fragility curves derived for the $LS2_T$ limit state for transverse sway-braced trapezes and the $LS1_{PJ}$ limit state for the suspended piping system piping joints are compared in Fig. 18. The fragility curves of the suspended piping system piping joints exhibit lower values of median PFA for corresponding probabilities of

Table 6
Parameter values of the fitted lognormal fragility curves for the transverse and longitudinal sway-braced trapezes.

Transverse sway-braced trapezes								
	Limit state 1 ($LS1_T$)				*Limit state 2 ($LS2_T$)*			
Archetype ID	*M1*		*M2*		*M1*		*M2*	
	θ (g)	β	θ (g)	β	θ (g)	β	θ (g)	β
1	0.47	0.46	0.47	0.46	1.13	0.54	1.13	0.54
2	0.24	0.55	0.42	0.65	0.41	0.53	0.90	0.67
3	0.18	0.52	0.38	0.70	0.33	0.46	0.75	0.51
4	0.18	0.50	0.38	0.70	0.33	0.48	0.75	0.50
5	0.31	0.66	0.31	0.66	0.92	1.22	0.92	1.22
6	0.11	0.43	0.15	0.43	0.23	0.44	0.38	0.40
7	0.10	0.58	0.09	0.50	0.17	0.73	0.28	0.48
8	0.11	0.48	0.12	0.64	0.20	0.60	0.31	0.41
Longitudinal sway-braced trapezes								
	Limit state 1 ($LS1_T$)				*Limit state 2 ($LS2_T$)*			
Archetype ID	*M1*		*M2*		*M1*		*M2*	
	θ (g)	β	θ (g)	β	θ (g)	β	θ (g)	β
1	0.74	0.48	0.74	0.48	N.E.	N.E.	N.E.	N.E.
2	0.32	0.62	0.69	0.67	0.61	0.33	1.09	0.41
3	0.27	0.53	0.66	0.71	0.51	0.35	0.83	0.30
4	0.27	0.53	0.67	0.71	0.51	0.34	0.84	0.27
5	0.49	1.23	0.49	1.23	0.81	0.32	0.81	0.32
6	0.17	0.40	0.20	0.50	0.49	0.30	0.53	0.24
7	0.15	0.66	0.17	0.47	0.44	0.37	0.43	0.31
8	0.15	0.54	0.16	0.59	0.42	0.26	0.40	0.36

Table 7
Parameter values for the fitted lognormal fragility curves for the piping joints of the suspended piping system.

Piping joints				
	Limit state 1 ($LS1_{PJ}$)			
Archetype ID	*M1*		*M2*	
	θ (g)	β	θ (g)	β
1	0.88	0.58	0.92	0.64
2	0.31	0.69	0.69	0.91
3	0.25	0.63	0.63	1.03
4	0.25	0.63	0.62	1.00
5	0.57	1.29	0.57	1.28
6	0.16	0.66	0.21	0.81
7	0.16	0.65	0.17	0.73
8	0.17	0.60	0.19	0.68

Table 8
Fundamental period (T_{1SP}) of the suspended piping archetypes modelled by neglecting the response of the hangers (M1) and assuming an EPP response (M2).

Archetype ID	*T_{1SP} (s)*	
	M1	*M2*
Archetypes with branches		
1	0.23	0.23
2	0.30	0.25
3	0.31	0.26
4	0.31	0.26
Archetypes without branches		
5	0.28	0.28
6	0.36	0.35
7	0.41	0.40
8	0.50	0.46

exceedance than that of the transverse sway-braced trapezes, indicating that for most of the cases considered, leakage will occur through the piping joints before the transverse sway-braced trapezes experience failure in the majority of the cases. However, for the suspended piping archetypes designed with values of the behaviour factor q_a equal to 3 and 4, and using the EPP modelling approach, the fragility curves derived for the $LS2_T$ and $LS1_{PJ}$ limits states intersect, meaning that for low values of the median PFA leakage through the piping joints will take place before the transverse sway-braced trapezes experience failure, while for larger median PFA values the transverse sway-braced trapezes will fail before leakage occurs through the piping joints. These results are consistent with observations from recent seismic events [4,5].

An important observation that can be made based on the derived fragility curves, is that for the studied archetypes, designing the suspended piping systems for lower values of the behaviour factor q_a results in a better seismic performance of the system regardless of the modelling approach considered for the hangers. As it can be seen in Eq. (5), the required spacing of the sway-braced trapezes s_a is directly proportional to the behaviour factor q_a. Therefore, designing the suspended piping systems for lower values of the behaviour factor q_a reduces the required spacing of the sway-braced trapezes s_a, which translates into a higher lateral stiffness of the system. Some design provisions, for example the NFPA 13 for fire-sprinkler systems, specifies maximum spacing requirements for the lateral bracing of suspended piping systems. In the current edition of Eurocode 8 seismic provisions, no such requirements are specified. The effect of implementing maximum spacing requirements for the lateral bracing of suspended piping systems in their seismic performance should be further studied using a larger number of building and suspended piping system archetypes, and it is out of the scope of this investigation.

Finally, from the derived fragility curves it can be concluded that the decision to neglect the dynamic response of the hangers in the seismic design and analysis of suspended piping systems may be conservative, given that when implementing the EPP modelling approach for the hangers, an improved seismic performance was observed for most suspended piping archetypes. However, the modelling approach assumed in this study for the hangers was based solely on material and geometric properties available from the product manufacturer [30], given that to the authors knowledge, there is currently no information in the public literature regarding seismic performance parameters of suspended piping hangers. The results obtained in this study highlight the importance of conducting component testing of suspended piping hangers, to obtain reliable performance parameters that can be used to calibrate numerical models.

6. Conclusions

This paper presented the results of a parametric numerical study to investigate the influence of the gravity load trapezes (hangers) on the overall seismic performance of suspended piping systems. The main objective of this study was to evaluate the common assumption of neglecting the contribution of the gravity load trapezes on the overall seismic performance of suspended piping systems. Two different suspended piping layouts to be installed in four different moment-resistant frames (MRFs) designed according to Eurocode 8 seismic provisions for a medium-to-high seismicity site in Europe were selected for this investigation. A cascading analysis approach was implemented to estimate the seismic demand that the selected suspended piping layouts would experience in the various supporting structures. Non-linear time history analysis (NLTHA) of the four selected MRFs was conducted following a multiple stripe approach using nine sets of ground motion record pairs of increasing seismic hazard intensity selected according to the conditional mean spectrum method. The results of these analyses were used to create a database of roof-level floor accelerogram pairs to be used to conduct bidirectional NLTHAs of the selected piping layouts.

The two selected piping layouts were designed according to Eurocode 8 seismic provisions by assuming four different values of the behaviour factor q_a (1, 2, 3 and 4, respectively) and calculating the corresponding spacing of the transverse and longitudinal sway-braced trapezes. This resulted in eight different suspended piping index archetypes. Non-linear numerical models of the archetypes were devel-

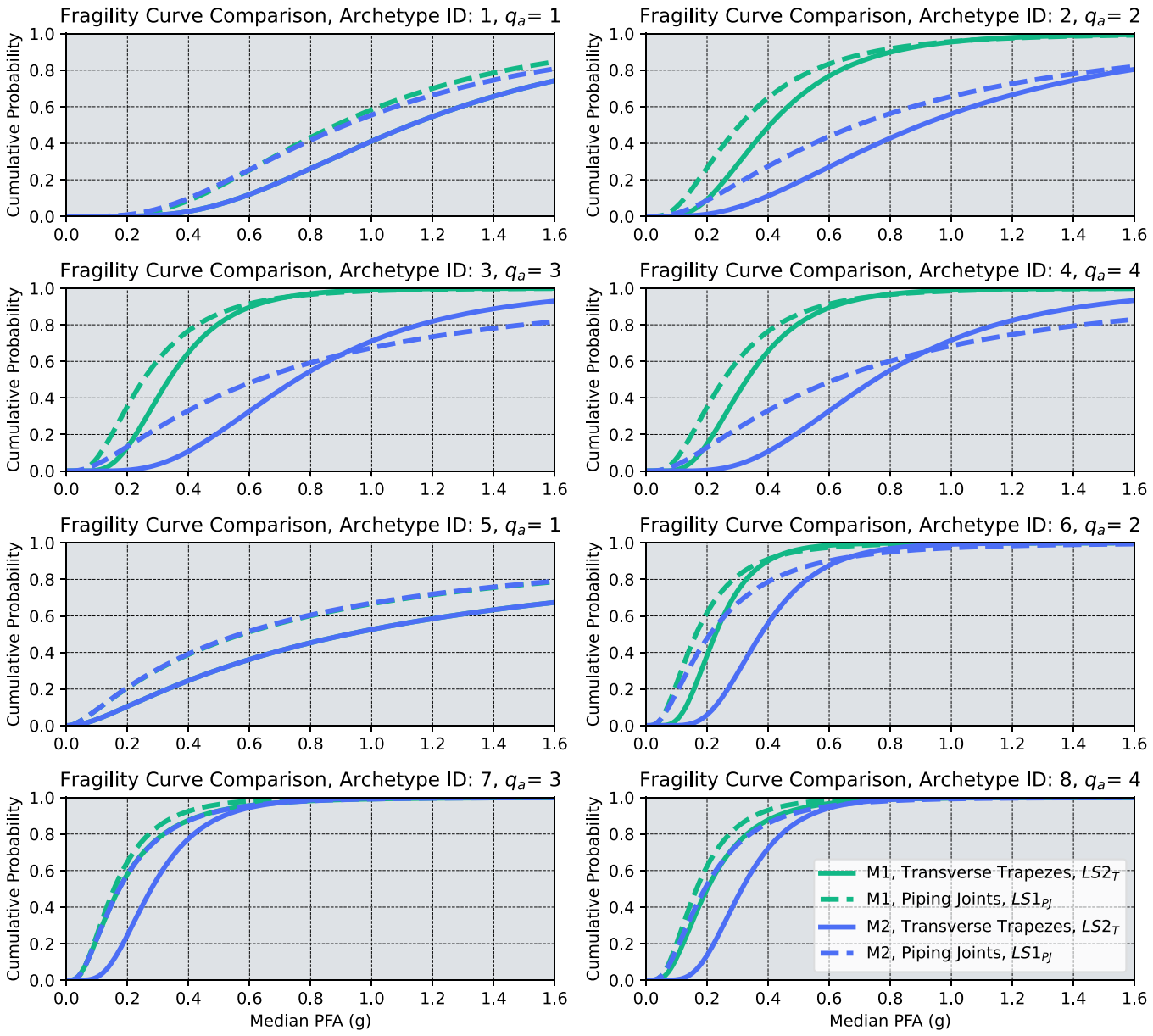

Fig. 18. Comparison of the fragility curves derived for the transverse sway-braced trapezes and the suspended piping system piping joints.

oped in the open-source platform OpenSees for two different approaches to model the suspended piping hangers: i) neglecting the contribution (and therefore, the lateral stiffness) of the hangers, and ii) modelling the hangers using elastic-perfectly plastic springs with an initial stiffness calculated according to the material and geometric properties reported by the product manufacturer, and an ultimate deformation estimated from experimental testing of suspended piping restraint installations. The modelling of the transverse and longitudinal sway-braced trapezes, and the piping joints was conducted by using non-linear springs calibrated based on results from experimental campaigns.

Based on the results of NLTHAs, lognormal fragility curves were derived independently for the transverse and longitudinal sway-braced trapezes, and the piping joints of the suspended piping archetypes using a multiple-stripe approach. In the case of the transverse and longitudinal sway-braced trapezes, the derivation of the fragility curves was conducted by using the displacement ductility demand as the engineering demand parameter (EDP) and median peak floor acceleration (PFA) of each seismic hazard intensity level as the intensity measure (IM) for two different limit states. For the piping joints, on the other hand, the fragility curves were derived using the leakage rotation ratio as the EDP and the median PFA of each seismic hazard intensity level as the IM for a single limit state.

By comparing the obtained fragility curves, it was observed that considering the contribution of the hangers in the numerical modelling of the suspended piping archetypes improved significantly their seismic performance in all the considered limit states. This could be interpreted as that the decision of neglecting the contribution of the hangers in the seismic design and analysis of suspended piping systems may be conservative. Furthermore, the obtained fragility curves show that the leakage through the piping joints was the dominating limit state in the overall performance of the suspended piping archetypes, which is consistent with field observations following recent seismic events.

One limitation of this research is that the elastic-perfectly plastic model implemented in this investigation for the numerical modelling of the hangers was based solely on the material and geometrical properties specified by the product manufacturer, given that to the authors' knowledge, there is currently no information available in the public literature regarding seismic performance parameters of suspended

piping hangers. The findings from this research underscore the necessity of conducting component tests on suspended piping hangers to establish reliable performance metrics that can be utilized to calibrate more detailed numerical models. Finally, it is important to highlight that in the case of seismic performance assessment of suspended piping systems, neglecting the contribution of the hangers could result in unrealistic seismic performances depending on the target performance objective, which reaffirms the importance of accounting for their contribution in the overall seismic performance of suspended piping systems.

CRediT authorship contribution statement

Filiatrault Andre: Writing – review & editing, Supervision, Project administration, Methodology, Funding acquisition, Conceptualization. **Perrone Daniele:** Writing – review & editing, Supervision, Project administration, Methodology, Funding acquisition. **Rodriguez Derek:** Writing – original draft, Validation, Software, Methodology, Investigation, Formal analysis, Conceptualization.

Declaration of Competing Interest

The authors declare the following financial interests/personal relationships which may be considered as potential competing interests: Derek Rodriguez reports financial support was provided by The Laboratories University Network of Seismic Engineering. Daniele Perrone reports financial support was provided by The Italian Ministry of Education, University and Research. If there are other authors, they declare that they have no known competing financial interests or personal relationships that could have appeared to influence the work reported in this paper.

Acknowledgements

The authors gratefully acknowledge the support of “The Laboratories University Network of Seismic Engineering” (RELUIS) thanks to the research project DPC-RELUIS 2022–2024. The second author gratefully acknowledges the funding by The Italian Ministry of Education, University and Research (PRIN Grant n. 2020YKY7W4, ENRICH Project).

Data Availability

Data will be made available on request.

References

[1] O’Reilly GJ, Perrone D, Fox M, Monteiro R, Filiatrault A. Seismic assessment and loss estimation of existing school buildings in Italy. Eng Struct 2018;168:142–62. https://doi.org/10.1016/j.engstruct.2018.04.056.
[2] Sousa L, Monteiro R. Seismic retrofit options for non-structural building partition walls: impact on loss estimation and cost-benefit analysis. Eng Struct 2018;161:8–27. https://doi.org/10.1016/j.engstruct.2018.01.028.
[3] Deierlein GG, Krawinkler H, Cornell CA. A framework for performance-based earthquake engineering. Pac Conf Earthq Eng 2003;2003.
[4] Miranda E, Mosqueda G, Retamales R, Pekcan G. Performance of nonstructural components during the 27 February 2010 Chile earthquake. Earthq Spectra 2012;28:453–71. https://doi.org/10.1193/1.4000032.
[5] OSHPD. The Northridge earthquake: a report to the hospital building safety board on the performance of hospitals. Sacramento, CA, U.S.: Official of Statewide Health Planning and Development, Facilities Development Division; 1995.
[6] Perrone D, Filiatrault A, Peloso S, Brunesi E, Beiter C, Piccinin R. Experimental seismic response evaluation of suspended piping restraint installations. Bull Earthq Eng 2020;18:1499–524. https://doi.org/10.1007/s10518-019-00755-5.
[7] Perrone D, Brunesi E, Filiatrault A, Peloso S, Nascimbene R, Beiter C, et al. Seismic numerical modelling of suspended piping trapeze restraint installations based on component testing. Bull Earthq Eng 2020;18:3247–83. https://doi.org/10.1007/s10518-020-00832-0.
[8] Wood R, Hutchinson T, Hoehler M, Kreidl B. Numerical Model Development and Experimental Validation of Trapeze Assemblies Utilizing Modular Channel Systems. San Diego La Jolla: Department of Structural Engineering, University of California; 2013.
[9] Tian Y, Filiatrault A, Mosqueda G. Experimental seismic fragility of pressurized fire suppression sprinkler piping joints. Earthq Spectra 2014;30:1733–48. https://doi.org/10.1193/111011EQS278M.
[10] Tian Y, Filiatrault A, Mosqueda G. Seismic response of pressurized fire sprinkler piping systems II: numerical study. J Earthq Eng 2015;19:674–99. https://doi.org/10.1080/13632469.2014.994148.
[11] Blasi G, Perrone D, Aiello MA. Parametric investigation on the response of suspended piping systems to tri-directional seismic excitation. Eng Struct 2023;293:116713. https://doi.org/10.1016/j.engstruct.2023.116713.
[12] CEN. Eurocode 8: Design of structures for earthquake resistance - Part 1: General rules, seismic actions and rules for buildings, EN 1998-1 2004.
[13] McKenna F., Fenves G., Scott M. Open System for Earthquake Engineering Simulation; 2000.
[14] ASCE. Minimum Design Loads and Associated Criteria for Buildings and Other Structures, ASCE/SEI 7-22 2022.
[15] Hadjian AH, Ellison B. Decoupling of secondary systems for seismic analysis. J Press Vessel Technol 1986;108:78–85.
[16] Perrone D, Brunesi E, Filiatrault A, Nascimbene R. Probabilistic estimation of floor response spectra in masonry infilled reinforced concrete building portfolio. Eng Struct 2020;202:109842. https://doi.org/10.1016/j.engstruct.2019.109842.
[17] Priestley M, Calvi GM, Kowalsky M. Displacement-based seismic design of structures. Pavia: IUSS Press, Istituto Universitario di Studi Superiori di Pavia; 2007.
[18] Stucchi M, Meletti C, Montaldo V, Crowley H, Calvi G, Boschi E. Seismic hazard assessment (2003-2009) for the Italian building code. Bull Seismol Soc Am 2011;101:1885–911. https://doi.org/10.1785/0120100130.
[19] NTC18. Nuove Norme Techniche per le Costruzioni (NTC18); 2018. .
[20] Woessner J, Laurentiu D, Giardini D, Crowley H, Cotton F, Grünthal G, et al. The 2013 European Seismic Hazard Model: key components and results. Bull Earthq Eng 2015;13:3553–96. https://doi.org/10.1007/s10518-015-9795-1.
[21] University of California, Berkeley. PEER NGA-West Dataset; 2008.
[22] Jayaram N, Lin T, Baker JW. A computationally efficient ground-motion selection algorithm for matching a target response spectrum mean and variance. Earthq Spectra 2011;27:797–815. https://doi.org/10.1193/1.3608002.
[23] Tatarsky M, Filiatrault A. Seismic response of viscously damped thin-wall piping system: a proof-of-concept case study. Bull Earthq Eng 2018. https://doi.org/10.1007/s10518-018-0447-0.
[24] NFPA. NFPA 13, Standard for the Installation of Sprinkler Systems; 2022.
[25] Perrone D, Rodriguez D, Filiatrault A, Brunesi E, Beiter C, Piccinin R. A framework for the quantification of non-structural seismic performance factors. J Earthq Eng 2022;26:8468–94. https://doi.org/10.1080/13632469.2021.1991516.
[26] Blasi G, Perrone D, Aiello MA, Pecce MR. Seismic performance assessment of piping systems in bare and infilled RC buildings. Soil Dyn Earthq Eng 2021;149:106897. https://doi.org/10.1016/j.soildyn.2021.106897.
[27] Soroushian S, Zagui AE, Echeverria A, Tian Y, Filiatrault A. Comprehensive analytical seismic fragility of fire sprinkler piping systems. Multidiscip Cent Earthq Eng Res 2014.
[28] DeGrassi G, Hofmayer C. Seismic analysis of simplified piping systems for the NUPEC ultimate strength piping test program. Washington, US: Division of Engineering Technology, Office of Nuclear Regulatory Research; 2005.
[29] Lee DG, Song YH. Efficient seismic analysis of piping systems with joint deformations. Eng Struct 1993:2–12.
[30] Hilti. European Technical Assessments: Fire Resistant Solutions for Modular Support Systems; 2021.
[31] Casto M. Personal communication. Technical Engineer, Hilti Italy 2024.
[32] Baker JW. Efficient analytical fragility function fitting using dynamic structural analysis. Earthq Spectra 2015;31:579–99. https://doi.org/10.1193/021113EQS025M.